Inorganic Chemistry

Article

pubs.acs.org/IC

Combined Theoretical and in Situ Scattering Strategies for Optimized Discovery and Recovery of High-Pressure Phases: A Case Study of the GaN–Nb_2O_5 System

William R. Woerner,[†] Guang-Rui Qian,[†] Artem R. Oganov,[†] Peter W. Stephens,[‡] H. A. Naveen Dharmagunawardhane,[§] Alexandra Sinclair,[∥] and John B. Parise*[,†,∥,⊥,#]

[†]Department of Geosciences, [‡]Department of Physics and Astronomy, [§]Department of Materials Science and Engineering, [∥]Mineral Physics Institute, and [⊥]Department of Chemistry, Stony Brook University, Stony Brook, New York 11794, United States

[#]Photon Sciences, Brookhaven National Laboratory, Upton, New York 11934, United States

Supporting Information

ABSTRACT: The application of pressure in solid-state synthesis provides a route for the creation of new and exciting materials. However, the onerous nature of high-pressure techniques limits their utility in materials discovery. The systematic search for novel oxynitrides—semiconductors for photocatalytic overall water splitting—is a representative case where quench high-pressure synthesis is useful and necessary in order to obtain target compounds. We utilize state of the art crystal structure prediction theory (USPEX) and in situ synchrotron-based X-ray scattering to speed up the discovery and optimization of novel compounds using high-pressure synthesis. Using this approach, two novel oxynitride phases were discovered in the GaN–Nb_2O_5 system. The $(Nb_2O_5)_{0.84}$:$(NbO_2)_{0.32}$:$(GaN)_{0.82}$ rutile structured phase was formed at 1 GPa and 900 °C and gradually transformed to a α-PbO_2-related structure above 2.8 GPa and 1000 °C. The low-pressure rutile type phase was found to have a direct optical band gap of 0.84 eV and an indirect gap of 0.51 eV.

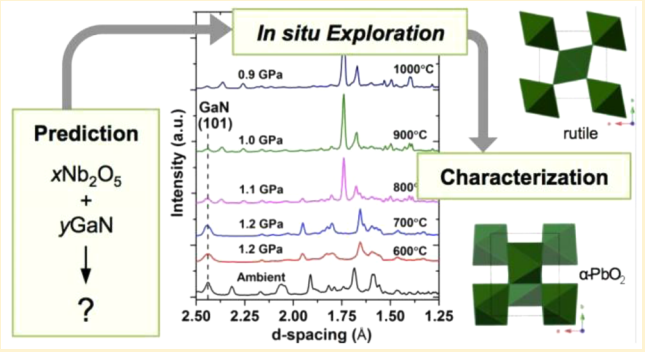

INTRODUCTION

High-pressure (HP) synthesis is underutilized relative to exploratory solid-state chemical synthesis at ambient pressure.[1−3] Despite its perceived specialist nature, "pressure tuning",[4] along with serendipitous[5] and theory-guided strategies,[6] provides exciting avenues for the discovery of novel solid-state materials at high pressures. The specialized infrastructure that is required, however, along with the slow throughput implied by the need to perform individual quench experiments to explore high-pressure and high-temperature (HPHT) phase space, conspires to limit the use of HPHT exploratory synthesis.[3] Exhaustive coverage of pressure–temperature (P-T) space requires months of work using "cook-and-look" quench recovery tactics. On the other hand, recent successes in producing novel materials inspired by theory[7−12] suggest collaborations employing crystal structure prediction to identify P-T conditions under which a target phase is stable, in combination with in situ observation of reactions at synchrotron and neutron sources,[11,13] will facilitate and expedite HP materials discovery in the future.

The problem of crystal structure prediction is central to the rational design of functional materials and is among the most complex problems in solid-state inorganic chemistry. Historically, computational methods have been ineffective in predicting reaction conditions and the structure of inorganic solids, and commentary on this problem has ranged from labeling it a "scandal",[14] to the somewhat more helpful suggestion that, although we cannot not as yet proceed ab initio from the desired property to a functional material, we can proceed incrementally toward this goal.[15] In the decades since such commentaries, there has been sustained and fruitful progress in computational materials discovery, which include fully nonempirical global optimization searches, such as employed by the USPEX method,[10,16] and data mining techniques.[17−19] These two approaches are quite complementary, especially in the case of ambient-pressure synthesis. However, strategies relying on database searching and algorithms for substituting anions and cations into known structures are of a more limited utility on application to potential high-pressure phases, as empirical knowledge is sparse and HP chemistry can be very different from that under ambient conditions.[6,18,20] The ab initio evolutionary algorithm embodied in the USPEX method, on the other hand, is computationally more expensive but can be applied without depending on the availability of pre-existing empirical knowl-

Received: December 1, 2015
Published: March 22, 2016

DOI: 10.1021/acs.inorgchem.5b02791
Inorg. Chem. 2016, 55, 3384−3392

edge and therefore is capable of predicting totally new and unexpected crystal structures and chemical compositions.

Oxynitrides: Anticipated Advantages of High-Pressure Synthesis. Oxynitride compounds have shown a wide array of properties and applications, which include pigments, dielectrics, magneto resistance, and photocatalysis.[21] Oxynitrides of d^{10} and d^0 cations have garnered significant interest in recent years due to their potential to act as overall visible light water splitting photocatalysts.[22] Water splitting photocatalysts need to have conduction and valence band positions that straddle the water reduction and oxidation potentials (1.23 V), to have a band gap small enough to absorb in the solar spectrum, and to remain chemically inert during the reaction.[22,23] Oxynitrides are desirable as photocatalysts, since they typically have band gaps narrower than those of the respective oxides while having higher air stability and corrosion resistance in comparison to nitrides.[22,23] The most notable and efficient system is the GaN−ZnO solid solution, which has shown the ability to split water under visible light irradiation with a quantum efficiency of 5.9%.[24] However, as the efficiency of known photocatalysts has yet to reach levels of commercial viability, research is focused on discovering new materials.

Typically, oxynitrides are synthesized via the ammonolysis of oxides at ambient pressure, but not all oxides will react at the moderate temperatures used during ammonolysis. The application of HP provides a route for direct solid-state oxynitride synthesis using oxide and nitride reagents, as pressure suppresses the decomposition of the nitride at high temperatures and enhances the reactivity of reagents. Surprisingly, there are few examples of oxynitrides synthesized using HP methods. Examples of successful recovery experiments include $LiNbO_3$-type $MnTaO_2N$ at 6 GPa,[25] $BaNbO_2N$, La_2AO_3N (A = Al, Nb, Ti, V) oxynitrides synthesized at 5 GPa,[26] $RZrO_2N$ (R = Pr, Nd, Sm) synthesized at 2−3 GPa,[27] the spinel-structured Ga_3O_3N at pressures between 1 and 5 GPa,[28−31] the wurtzite-structured GaN−ZnO solid solution at pressures between 1.7 and 6.2 GPa,[32] moganite-type PON prepared at 2.5 GPa,[33] and δ-PON prepared at 12.5 GPa.[34] High-pressure synthesis is an underutilized tool in oxynitride synthesis and is perhaps an important complement to the accessible ammonolysis route.

Using Crystal Structure Prediction To Guide Oxynitride Synthesis. The USPEX approach has had great success in predicting HP phases that were subsequently confirmed experimentally.[11,12,35−37] The current version (9.4.3) of USPEX features HP variable-composition structure prediction that utilizes the mixing of end member chemistries,[9] with the fitness function defined through the thermodynamic convex hull construction. This approach has been used, for example, to investigate the stability of new stoichiometries in the systems of Fe−C, Fe−H,[38] Hf−C,[39] Na−Cl,[6] Xe−O,[40] Mg−O,[41] W−B,[42,43] and HfO_2−SiO_2.[44] Experimental results confirmed the existence of the predicted $NaCl_3$ and Na_3Cl phases[6] as well as WB_3 and WB_{3+x} phases.[42]

Accurate structure prediction using USPEX presents some challenges for HP oxynitride compounds. As nitrogen and oxygen have similar ionic sizes, coordination numbers, polarizabilities, and electronegativities, these anions can be disordered across anion sites.[21] While some oxynitride compounds exhibit partial ordering,[45−49] ideally ordered oxynitrides are rarely encountered and include the only natural mineral oxynitride sinoite (Si_2N_2O)[50,51] and the TaON photocatalyst.[52] UPSEX performs ground-state calculations only on ordered structures, as occupational disorder would increase the computation cost by several orders of magnitude. Including temperature and configurational entropy can result in a different structure type and a shift of the transition pressure, in comparison to 0 K. USPEX does, however, provide a useful guide, identifying compositions likely to lead to thermodynamically stable materials.

Herein, we describe a method combining theoretical and experimental techniques to allow for more efficient discovery of novel materials at high pressures. In order to ameliorate the major problems with HP-materials discovery and sample optimization, we developed new approaches that combine modern computational tools, in situ observation of reactions with X-ray diffraction while varying P-T, and structural characterization. To test these approaches, we choose to focus on the formation of novel d^0/d^{10} mixed oxynitrides in the GaN−Nb_2O_5 system, as the system has the potential to form compounds with photocatalytic properties.

EXPERIMENTAL SECTION

USPEX Calculations. Using the evolutionary algorithm as implemented in USPEX,[53−55] a variable-composition search was performed to generate a range of compounds with initial chemical compositions chosen at random from a mixing of GaN and Nb_2O_5 endmembers. This population of structures, and their compositions, then evolved with the help of variation operators (among which, transmutation and heredity are composition-changing, and lattice mutation and soft-mode mutation are composition-conservative). All of the generated structures were relaxed and then ranked according to their fitness, with only the fittest 60% of each generation allowed to produce the next generation of structures. The underlying ab initio structure relaxation and electronic structure calculations were carried out using the all electron projected augmented wave (PAW) method[56] as implemented in the Vienna ab initio simulation package (VASP).[57] The Perdew−Burke−Ernzerhof (PBE) functional was used to treat the exchange-correlation energy.[58] A plane-wave kinetic cutoff energy of 600 eV was used in addition to reciprocal space sampling with dense Monkhorst−Pack *k*-point meshes[59] at a resolution of $2\pi \times 0.05$ Å^{-1} in order to provide sufficient accuracy during enthalpy calculations.

GaN Synthesis. The GaN used for this investigation was synthesized in house via the ammonolysis of Ga_2O_3 to ensure phase purity. A 2 g sample of Ga_2O_3 (99.99%, Sigma-Aldrich) was loaded into a quartz boat and placed in a plugged quartz tube attached to vacuum and gas manifolds in a 1 in. diameter tube furnace. The atmosphere was evacuated to rough vacuum and then filled to 1 bar of pressure with ammonia gas. The Ga_2O_3 reacted with the ammonia flowing at a rate of 500 mL/min at 950 °C for 2 h. The product was cooled back to room temperature under flowing ammonia and was then removed, ground for 10 min in an agate mortar and pestle, and then subjected to the reaction conditions described above for a second time. X-ray diffraction (XRD) of the recovered pale yellow powder revealed that it consisted of nanocrystalline wurtzite-type GaN with no detectable Ga_2O_3.

In Situ HPHT XRD Investigation. The HPHT reaction of GaN−Nb_2O_5 was studied in situ at pressures and temperatures up to 3.8 GPa and 1200 °C using energy dispersive XRD (EDXRD) at the X17B2 beamline at the National Synchrotron Light Source (NSLS). A 1:1 mix of GaN and Nb_2O_5 (99.99%, Sigma-Aldrich) was mechanically ground in an agate mortar and pestle for 45 min and loaded into a BN sleeve. The mix was stacked on top of an MgO internal pressure standard and physically separated with a layer of BN powder. The sleeve was inserted into a boron epoxy cubic DIA cell with a resistive heating graphite furnace and a W-3%Re/W-28%Re thermocouple (Figure 4). The cell was compressed using a 1000 ton multianvil press (BAM11), and the EDXRD patterns were collected using a white beam (14−120 keV X-rays) incident on tungsten slits to produce a 100 μm × 100 μm beam. The cell was first compressed to a press loading of 15 tons (~1

DOI: 10.1021/acs.inorgchem.5b02791
Inorg. Chem. 2016, 55, 3384−3392

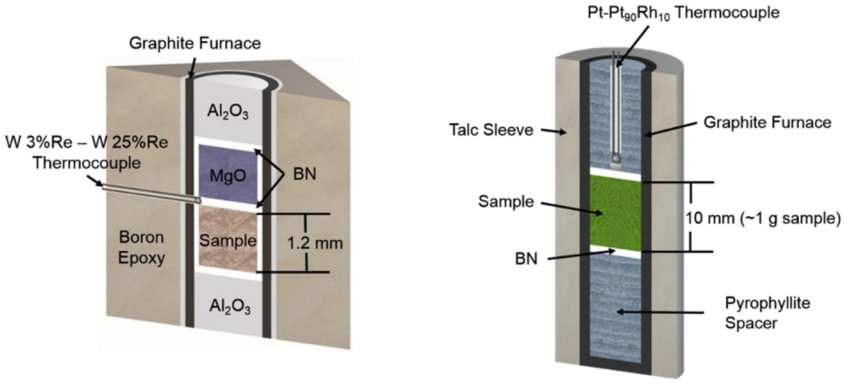

Figure 1. Cross section of the cubic cell assembly (left) used at the X17B2 beamline at NSLS and the 19 mm diameter piston cylinder cell assembly (right). The cubic assembly measures 6.35 mm on each side, and the overall length of the piston cylinder assembly is 4.45 cm.

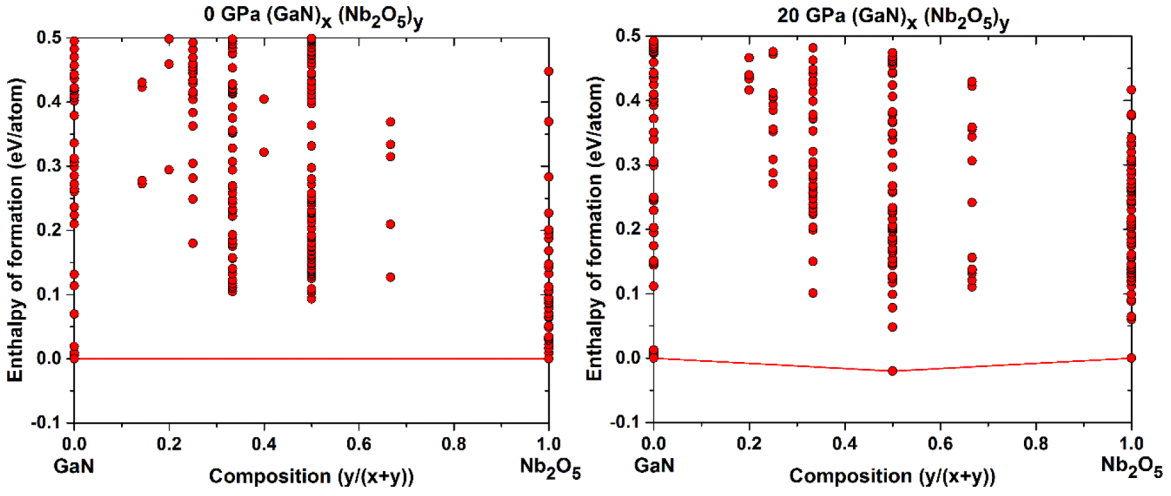

Figure 2. Predicted enthalpies of formation for GaN–Nb_2O_5 compounds at ambient pressure (left) and 20 GPa (right). The circles represent individual structures and are plotted as compositions versus enthalpies of formation.

GPa), and the temperature was raised to 1000 °C with EDXRD patterns collected every 100 °C with 300 s exposure after a 1000 s reaction time. The cell was then cooled to room temperature, followed by an increase in pressure to 25 tons. The temperature was then raised in 100 °C increments to 1200 °C with the same EDXRD data collection strategy described above employed at the end of each increment, with the process again repeated at 35 tons.

HPHT Piston Cylinder Quench Experiments. HPHT reactions between GaN and Nb_2O_5 were carried out ex situ using a piston cylinder apparatus at P-T points selected according to the phase stability fields determined from the in situ EDXRD results. For the 1 GPa experiment, a 19 mm (0.75 in.) diameter piston cylinder setup was used to maximize the sample volume. Approximately 1 g of the GaN–Nb_2O_5 mix was loaded in a graphite furnace and encapsulated within the cylinder with two BN disks. The sample was centered in the furnace using two pyrophyllite plugs that were previously fired at 1000 °C for 20 min. The temperature was monitored with a Pt/Pt_{90}-Rh_{10} thermocouple pressed against the BN disk just above the sample in the talc cell assembly (Figure 1). The entire assembly was cold-compressed to the desired pressure and ramped up to temperature while the pressure was held constant. The mixtures were left to react for 1 h and then quenched isobarically. For the 3 GPa quench experiment, a 12.7 mm (0.5 in.) diameter piston cylinder assembly was used, as the 19 mm diameter assembly could not reach such high pressures. The 12.7 mm diameter cell assembly is a scaled-down version of what is shown in Figure 4, with a substitution of alumina for pyrophyllite plugs. However, only about 50–100 mg of the mix can be loaded in such an assembly. After decompression, the sample pellets were removed from the assembly and physically cleaned to remove any contamination from the cell assembly before grinding.

Analytical Methods. The quenched samples were initially characterized with powder XRD using a Rigaku Ultima IV (CuKα) with a D/Tex linear position sensitive detector in Bragg–Brentano geometry. After phase identification and comparison with in situ EDXRD patterns, the crystalline powders were structurally characterized using synchrotron high-resolution XRD and the 1 GPa sample was additionally investigated with time-of-flight (TOF) powder neutron diffraction. High-resolution powder XRD investigations were carried out at the 11-BM beamline at the Advanced Photon Source. The high-resolution XRD patterns were collected with a wavelength of 0.41383(1) Å at room temperature while the samples were spun on a goniometer in a Kapton capillary. The patterns were collected over an angular range of $0.8° \leq 2\theta \leq 49.99°$ with a step size of 0.001°. The TOF powder neutron diffraction experiment was conducted using the POWGEN instrument (BL-11) at the Spallation Neutron Source. Approximately 1 g of sample was loaded into a 6 mm vanadium can, and data were collected using frames 1 and 5 (chopper wavelength centered at 0.533 and 3.731 Å, respectively), giving access to a range of 0.25 Å $\leq d \leq$ 6 Å. Diffuse reflectance spectra were collected using an ASD Fieldspec3Mac UV–vis–NIR spectrometer with an Ocean Optics HL-2000-HP tungsten halogen light source. Compositional analysis with inert gas fusion (for O and N) and direct current plasma emission spectroscopy (for Ga and Nb) was carried out by Luvak inc., Boylston, MA.

DOI: 10.1021/acs.inorgchem.5b02791
Inorg. Chem. 2016, 55, 3384–3392

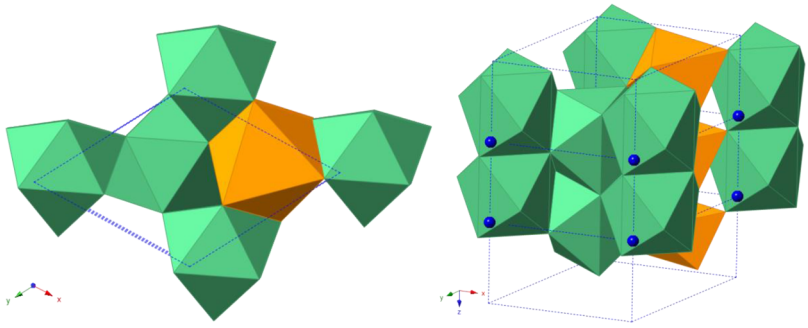

Figure 3. Lowest energy $GaNb_2O_5N$ structure predicted to be stable at 20 GPa. Gallium (orange) is coordinated by six oxygen atoms in a distorted-octahedral geometry, while niobium (green) is coordinated by seven oxygen atoms and two nitrogen atoms in a tricapped-trigonal-prismatic geometry. The unit cell is outlined with a dashed blue line.

RESULTS

GaN−Nb_2O_5 USPEX Calculations. Variable-composition structure prediction calculations in the $(GaN)_x-(Nb_2O_5)_y$ system were performed at 0 and 20 GPa to evaluate the stability of the oxynitride compounds encountered. While the commercial zone of high pressure is most desirable (<6 GPa) for potential in scale-up production, the calculations need to be conducted at a significant overpressure to compensate for the 0 K temperature of the calculations. At 0 GPa, the calculations indicate that all of the predicted compounds are unstable and decomposition into the endmembers wurtzite GaN and R-Nb_2O_5 is energetically favored (Figure 2, left). However, calculations at 20 GPa indicate a stable oxynitride with a composition of $GaNb_2O_5N$, as the enthalpy of formation is lower than that of the end members wurtzite GaN and Z-Nb_2O_5 (Figure 2, right). The structure of the predicted ordered $GaNb_2O_5N$ phase is shown in Figure 3. The 20 GPa calculations indicate a high probability of a reaction occurring at HP, although the predicted structure did not match that of either of the oxynitride phases found in the HPHT experiments, described below.

In Situ HPHT EDXRD. The EDXRD results of the in situ HPHT reaction study conducted at the X17B2 beamline at the National Synchrotron Light Source are summarized in Figures 4−6. At approximately 1 GPa, we observe the onset of a reaction between GaN and Nb_2O_5 at 800 °C, as noted by a complete restructuring of the XRD pattern and a diminishment of the (101) GaN reflection (Figure 4); the reaction is complete by 1000 °C. The new Ga−Nb oxynitride observed at ∼1 GPa has major reflections in the EDXRD patterns at approximately 1.74 (211) and 1.64 Å (220), consistent with a rutile-type (TiO_2) structure (described below). At ∼2.8 GPa and 900 °C, the intensity of peaks attributed to the rutile-type phase begin to diminish as new reflections belonging to a α-PbO_2 type structure appear, indicative of a phase transition (Figure 5). Moreover, as the sample temperature is increased past 800 °C at 3−4 GPa, the phase transition continues with an increasing intensity of the α-PbO_2 reflections but without the complete disappearance of reflections attributable to the rutile-type phase (Figure 6).

The EDXRD patterns of the in situ HPHT investigation revealed that two novel oxynitride phases exist in the GaN−Nb_2O_5 system below 3.8 GPa and 1200 °C. The EDXRD patterns indicate that the optimal conditions for the quench synthesis of the rutile- and α-PbO_2-type phases are 1 GPa and 1000 °C and 3.8 GPa and 1200 °C, respectively. As the piston−cylinder apparatus is limited to $P \leq 3$ GPa, the quench

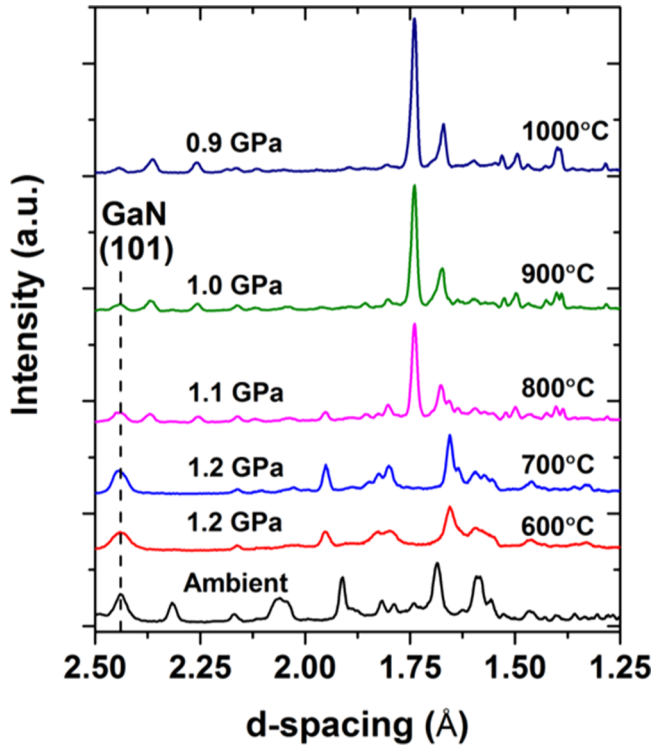

Figure 4. In situ EDXRD patterns of a 1:1 mixture of GaN and Nb_2O_5 at a constant press loading of 15 tons. The EDXRD pattern of the initial GaN:Nb_2O_5 mixture at ambient pressure and temperature is shown at the bottom of the figure in black and contains peaks attributed to only wurtzite-type GaN and monoclinic Nb_2O_5. When the sample was pressed to 1.2 GPa and heated to 600 and 700 °C, the Nb_2O_5 underwent a phase transformation to the orthorhombic phase but did not react. At ∼800 °C, however, the XRD pattern underwent a drastic change indicative of a reaction, highlighted by the decrease in intensity for the major GaN (101) refection as the rutile-structured oxynitride phase forms. The reaction is essentially complete by 1000 °C, with only minor GaN left unreacted.

experiment targeting the α-PbO_2 phase was conducted at 3 GPa and 1200 °C in order to maximize the amount of this phase in the sample.

The in situ studies of the GaN−Nb_2O_5 reaction mapped the phase stability in the P-T space and provided the optimal reaction temperatures for synthesis, thereby limiting the number of quench experiments required to recover the high-pressure phases to two. This represents a considerably higher success rate than could be realized from the use of single P-T

DOI: 10.1021/acs.inorgchem.5b02791
Inorg. Chem. 2016, 55, 3384−3392

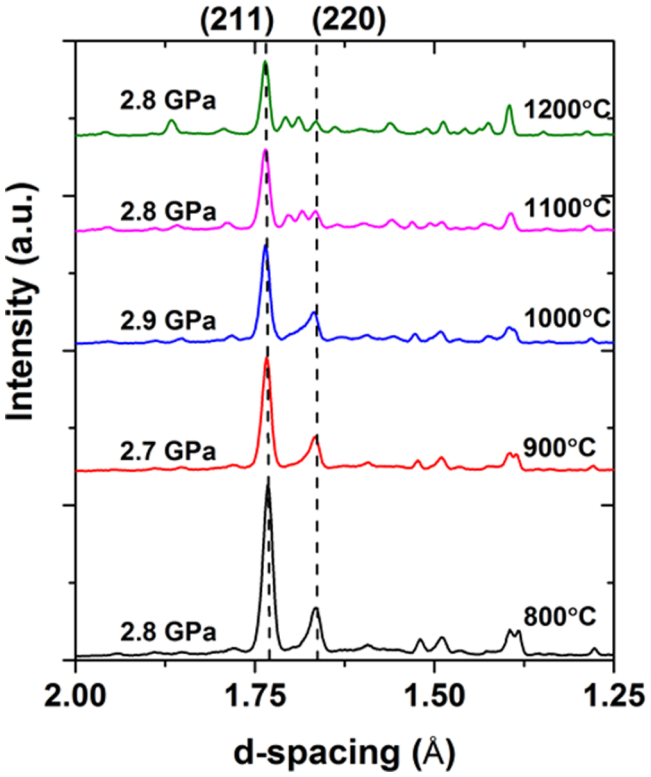

Figure 5. In situ EDXRD patterns of the GaN−Nb_2O_5 reaction at a constant press loading of 25 tons. The rutile oxynitride phase remains the only Ga−Nb oxynitride phase in the pattern as the sample is heated to 800 °C. At 900 °C, the intensity of the rutile-type (211) and (220) reflections begins to decrease and new peaks in the pattern are apparent by 1200 °C, belonging to the new α-PbO_2-type oxynitride phase.

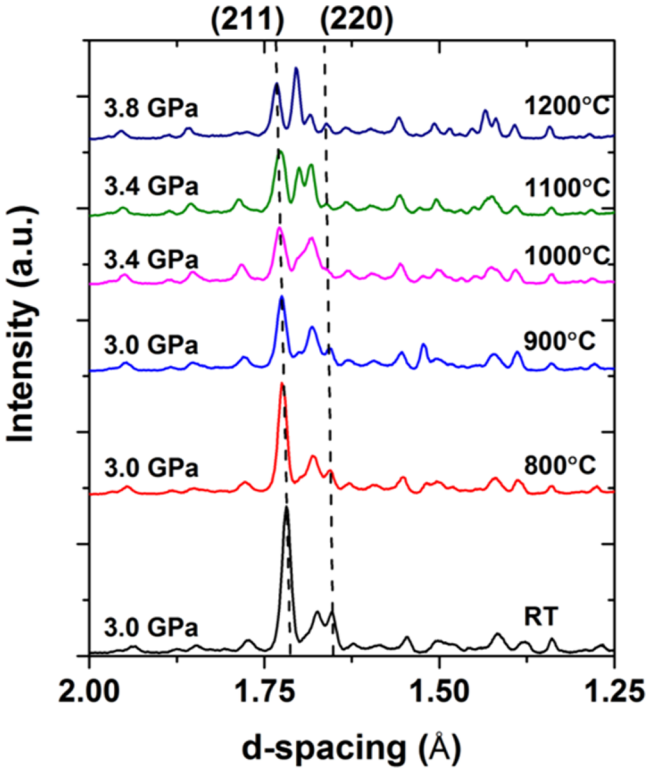

Figure 6. In situ EDXRD patterns of the GaN−Nb_2O_5 reaction at a constant press loading of 35 tons. Following the trend at 25 tons, as the temperature is increased, we see a decrease in the intensity of the rutile-type phase (211) and (220) reflections and the new peaks belonging to the α-PbO_2 -type phase increase in intensity through 1200 °C.

quench exploratory synthesis. Multianvil press assemblies at user facilities offer fast and extensive evaluation of reactions at industrially viable pressures and temperatures. Cell assemblies can also be made to house two different reactions with a pressure calibrant to speed up P-T exploration even further. With this experimental setup, two chemical systems can be evaluated up to modest pressures and temperatures (~5 GPa and 1500 °C) in a period of 24 h. The alternative process of conducting several quench-recovery experiments followed by the characterization of recovered phases to map P-T space could require weeks or months of work.

Structural Characterization. *1 GPa−1000 °C.* The product of the 1 GPa−1000 °C quench experiment was evaluated with both high-resolution XRD and TOF powder neutron diffraction. After the known phases were identified, the new oxynitride phase in the XRD pattern was indexed, its crystal structure solved, and a Rietveld refinement conducted with the program TOPAS (v4.1, Bruker AXS). The major phase is a new oxynitride found to have the rutile structure with minor GaN, $GaNbO_4$, and *T*-Nb_2O_5 also identified in the sample (Figure 7). The $GaNbO_4$ phase forms due to a Ga_2O_3 impurity in the reactant GaN powder (Figure S1 in the Supporting Information). Because of the large X-ray scattering contrast between Nb^{5+} and Ga^{3+}, the occupancies of $Nb^{5+}$and Ga^{3+} on the single metal site were refined, with the constraint that the total occupancy of the site is 1.0.

The X-ray scattering contrast between O^{2-} and N^{3-}, on the other hand, is small, and so neutron diffraction data were

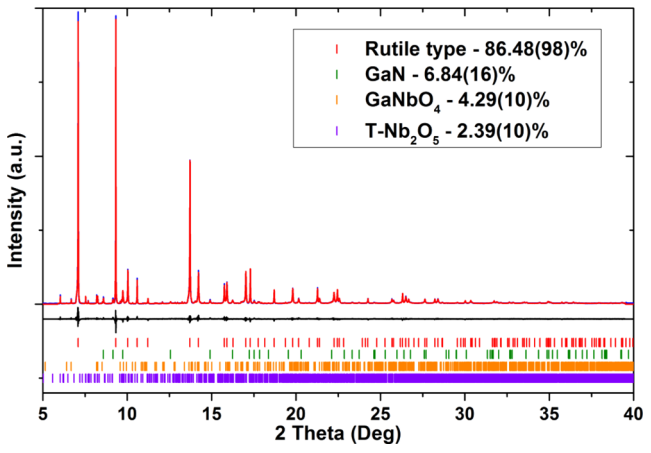

Figure 7. XRD Rietveld refinement result of the 1 GPa−1000 °C quench experiment. The collected pattern is shown in blue, the calculated pattern in red, and the difference in black. The tick marks show the positions of reflections of the respective phases; starting from the top, red markers represent positions for reflections from the rutile-type phase, green for GaN, brown for $GaNbO_4$, and purple for T-Nb_2O_5. Phase fractions are shown in weight percentages.

collected on the same sample as the neutron scattering contrast is high (b_O = 5.803 fm; b_N = 9.36 fm) and can resolve the O/N occupancy and any possible ordering on the anion site. A structure model was refined using two TOF frames and the GSAS/EXPGUI Rietveld software package (Figure 8).[60,61] As Nb^{5+} and Ga^{3+} have nearly identical neutron scattering lengths

DOI: 10.1021/acs.inorgchem.5b02791
Inorg. Chem. 2016, 55, 3384−3392

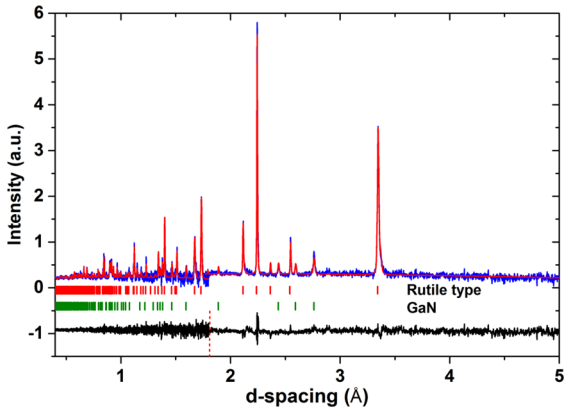

Figure 8. TOF powder neutron Rietveld refinement result of the 1 GPa−1000 °C synthesis. The patterns from both frames 1 (left) and 5 (right) are shown and are separated by the red dashed line in the difference pattern. The collected pattern is shown in blue, the calculated pattern in red, and the difference in black. The tick marks show the positions of reflections of the respective phases. The $GaNbO_4$ and T-Nb_2O_5 reflections were too weak to be incorporated into the refinement.

(b_{Nb} = 7.054 fm; b_{Ga} = 7.288 fm), the rutile-type metal site was fixed to the ratio determined from the XRD refinement. The occupancy of $O^{2-}$and N^{3-} on the anion site was allowed to freely refine (constrained to add up to 1). Using the refined occupancies on both the cation and anion sites, the chemical formula for the rutile-related phase is $Nb_{1.41}Ga_{0.58}O_{3.41}N_{0.59}$. To satisfy charge balance, this formula implies some reduction of Nb^{5+}, the existence of vacancies in the site occupied by Nb/Ga, or both. In the case of Nb^{5+} reduction, the composition may then nominally be represented as $(Nb_2O_5)_{0.84}$:$(NbO_2)_{0.32}$:$(GaN)_{0.82}$. No additional, superstructure peaks could be detected in either data set, indicating that both the anion and cation sites were indeed disordered.

The average composition of the sample synthesized at 1 GPa, calculated from Rietveld refinements and taking into account the phases which constitute it (Figure 7), is $Nb_{1.28}Ga_{0.72}O_{3.16}N_{0.67}$. Bulk chemical analysis yielded an average overall composition of $Nb_{1.26}Ga_{0.72}O_{3.56}N_{0.44}$ (see the Supporting Information), agreeing very well with Ga and Nb content calculated from refinements, though N and O contents were slightly different. We consider that, given the multiphase nature of the sample, the phase specific nature of the Rietveld refinement, and the scattering contrast between nitrogen and oxygen in particular, the composition obtained from the neutron refinement (Tables 1−3) gives an accurate measure of the nitrogen content of the rutile-related phase.

The refinement details and crystallographic data for the rutile-related phase is given in Table 1 (X-ray) and Table 2 (TOF neutron). The contents of Ga^{3+} and N^{3-}show excellent agreement between the two independent X-ray and neutron refinements, indicating that GaN directly reacts with Nb_2O_5 and the Ga_2O_3 component is ignored. A joint X-ray/neutron refinement was attempted using GSAS/EXPGUI, but the X-ray profile parameters could not model the peak shape well enough to enable a stable refinement. Structural details and selected bond lengths of both phases can be found in Tables 3 and 4, respectively.

3 GPa−1200 °C. The synthesis at 3 GPa−1200 °C yielded approximately 50 mg of sample used to collect a high-resolution powder XRD pattern. A Rietveld refinement using TOPAS revealed three phases to be present in the sample: a major rutile type and a minor α-PbO_2 type in addition to GaN (Figure 9).

Table 1. Summary of the Results of Rietveld Refinements using X-ray Data

	rutile type	α-PbO_2 type
pressure (GPa)	1	3
temp (°C)	1000	1200
space group	$P4_2/mnm$	$Pbcn$
a (Å)	4.72939(3)	4.63629(3)
b (Å)	4.72939(3)	5.59467(4)
c (Å)	3.02110(2)	4.97802(3)
V (Å^3)	67.573(1)	129.122(1)
R_p	0.9031	0.9468
R_{wp}	0.1188	0.1379
χ^2	1.628	1.513

Table 2. Neutron Rietveld Refinement Results for Rutile-Type Phase[a]

pressure (GPa)	1
temp (°C)	1000
space group	$P4_2/mnm$
a (Å)	4.7282(2)
b (Å)	4.7282(2)
c (Å)	3.0137(1)
V (Å^3)	67.373(5)
frame 1 R_p	0.1167
frame 1 R_{wp}	0.0799
frame 5 R_p	0.1366
frame 5 R_{wp}	0.1062
χ^2	1.621

[a]Data collected from sample synthesized by a quench experiment recovered from 1 GPa.

Table 3. Structure Details Determined for Refined Models using Neutron and X-ray[a]

atom	x	y	z	10^2U_{iso} (Å^2)
rutile Type (neutron)				
M	0.0	0.0	0.0	1.22(4)
A	0.2950(2)	0.2950(2)	0.0	1.19(3)
α-PbO_2 Type (X-ray)				
M	0.0	0.1749(2)	0.25	1.0(2)
A	0.269(1)	0.3864(7)	0.4201(9)	0.4(1)

[a]Refined site occupancies for the rutile-like phase. M occupancy: Nb = 0.71(1) and Ga = 0.29(1), determined from refinement using the X-ray data. A occupancy: O = 0.856(3) and N = 0.144(3), determined from refinement using the neutron data (see text).

Table 4. Selected Bond Distances (Å) of Oxynitride Phases

rutile type (neutron)	
M−A	1.972(2) × 4
	2.0372(8) × 2
M−M	3.01372(5)
α-PbO_2 type	
M−A	1.918(4) × 2
	1.989(4) × 2
	2.113(4) × 2
M−M	3.166(1)

DOI: 10.1021/acs.inorgchem.5b02791
Inorg. Chem. 2016, 55, 3384−3392

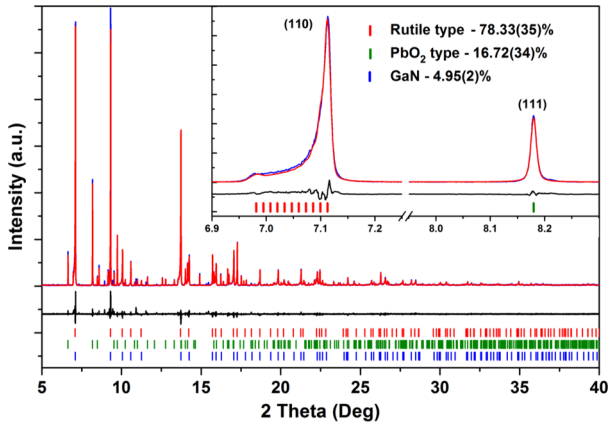

Figure 9. XRD Rietveld refinement result of a sample synthesized at 3 GPa−1200 °C and containing contributions to the diffraction pattern from a rutile-type phase, a α-PbO_2 type phase, and unreacted GaN. The collected pattern is shown in blue, the calculated pattern in red, and the difference in black. The vertical tick marks below the difference pattern show the positions of reflections of the respective phases; starting from the top, red markers represent positions for reflections from the rutile-type phase, green for α-PbO_2-type phase, and blue for GaN. The inset compares the largest reflection of the rutile type (110) with that of the α-PbO_2 type (111). For the (110) reflection there are 11 tickmarks belonging to the distribution of phases used to model variable composition of the rutile-type phase.

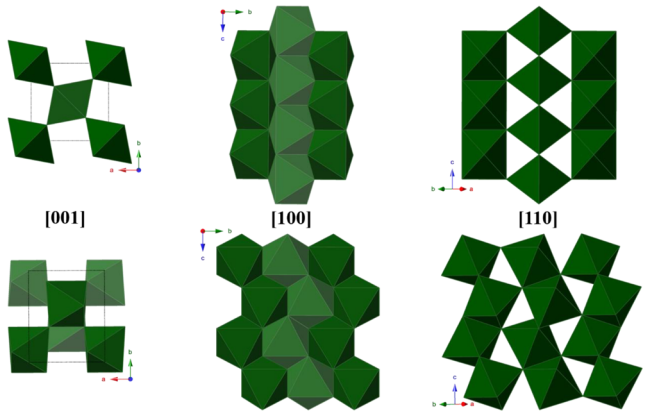

Figure 10. Crystal structures of rutile-type (top) and α-PbO_2-type oxynitride phases (bottom) in polyhedral representations.

The oxide phases of $GaNbO_4$ and Nb_2O_5 that were present in the lower pressure (1 GPa) sample are notably absent and have participated in the reaction at 3 GPa. The rutile-type phase in the sample has a large asymmetric peak shape likely due to chemical inhomogeneity during the slow phase transition to the α-PbO_2 type phase. The asymmetric peak shape of the rutile-type phase was modeled as 11 rutile phases, with a constrained distribution of tetragonal lattice parameters (Figure 9 inset), the scale factor for each phase was freely refined. See the Supporting Information for more information on the structure model. While the constrained multiphase approach did model the rutile type intensities well, the cation occupancy was globally set for the distribution of phases and allowed to refine. The occupancies of the individual rutile-type phases could not be refined due to the reflection overlap; therefore, the distribution of chemistries and the actual occupancy of Ga and Nb in these phases could not be accurately determined. With that caveat, trial refinements hinted at a difference between the rutile-type phases recovered in the 1 and 3 GPa samples. For example, while the 1 GPa sample contains a single rutile-related phase with Nb occupancy of ∼0.7 (Table 3), the fits of the distribution of rutiles in the 3 GPa sample suggested the same Nb occupancy of ∼0.55 across the whole distribution. This suggests that the inhomogeneity is predominantly in the O/N site and that this is changing as the lower pressure rutile phase gradually transforms to the high-pressure phase.

The chemistry of the α-PbO_2 type phase was set to that of the 1 GPa rutile phase and was not refined, because when the cation occupancy was left to freely refine, it was unstable and would converge at unrealistic ratios of Ga and Nb with no improvement to the refinement. The refinement and crystallographic details of the α-PbO_2 type phase are shown in Table 1. The crystal structure of the rutile-type phase is shown in comparison to the α-PbO_2 type in Figure 10.

The GaN−Nb_2O_5 system presents a worst-case scenario for evaluating crystal structure prediction theory as a guide for synthetic efforts. Apart from possible vacancies and multivalence of Nb, both anion and cation sites have the potential for considerable disorder. In oxides at 6-fold coordination, Ga^{3+} and Nb^{5+} have nearly identical ionic radii (Ga^{3+}, 0.62 Å; Nb^{5+}, 0.64 Å).[62] In retrospect, it is not surprising that the predicted structure does not match the experimental results, due to the high probability that configurational entropy would lower the Gibbs free energy of formation of new phases, with occupational disorder being possible between Ga^{3+} and Nb^{5+} as well as between N^{3-} and O^{2-}, which the current version of USPEX does not take into account. The USPEX calculations are useful, however, in guiding us to attempt a 1:1 mix of GaN and Nb_2O_5 and in correctly predicting that this composition is only synthesizable at high pressures.

Optical Properties of Rutile Type Oxynitride. The optical properties of the rutile-structured oxynitride were evaluated using UV−vis−NIR diffuse reflectance to determine whether the band gap was suitable for water splitting photocatalysis. The relative absorbance (α_{KM}) was generated using a Kubelka−Munk transform and was fit using the same band gap functional fitting methods used to study the optical properties of $(GaN)_{1-x}(ZnO)_x$ nanorods and nanocrystalline gallium oxynitride spinel.[63,64] The optical fitting revealed a contribution from a direct band gap of 0.84 eV as well as an indirect band gap of 0.51 eV (Figure 11).

The optical data and band gaps are consistent with the black color of the powder as it absorbs through the visible range. The short band gap is unexpected, as the respective oxide, $GaNbO_4$, is a wide band gap semiconductor.[65,66] However, a HPHT reaction of Ga_2O_3 and Nb_2O_5 under identical synthesis conditions (1 GPa, 1000 °C) produced a black powder of wolframite-type $GaNbO_4$ (Figure S2 in the Supporting Information).The color in both the HPHT oxide and the oxynitride is likely due to reduction of Nb^{5+} at the surface due to thermodynamically reducing conditions imposed by the graphite furnace.[67] Such a surface reduction occurs when rutile, TiO_2 (Ti^{4+} to Ti^{3+}), is heated under reducing atmospheres.[68] Synthesis under a less reducing atmosphere or postsynthesis oxidative treatment could change the color and perceived optical band gap. Unfortunately, in the as-synthesized state, the rutile-type phase with composition $Nb_{1.41}Ga_{0.58}O_{3.41}N_{0.59}$ is not suitable for photocatalytic water splitting.

DOI: 10.1021/acs.inorgchem.5b02791
Inorg. Chem. 2016, 55, 3384−3392

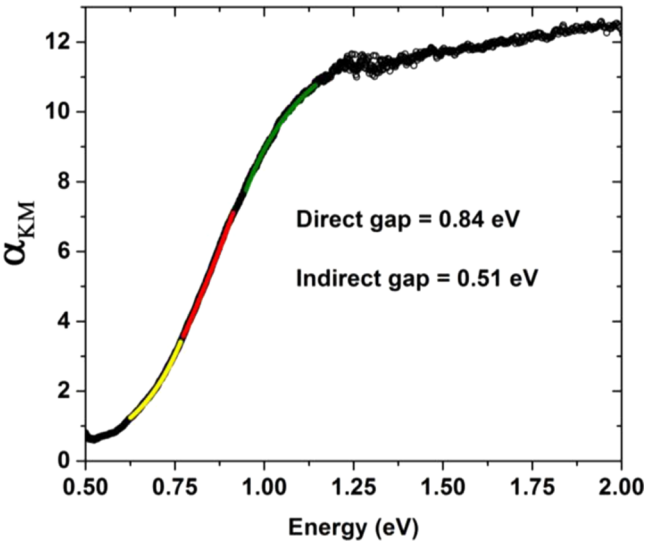

Figure 11. Kubelka–Munk absorption of the rutile-type phase synthesized at 1 GPa–1000 °C. The absorbance regions are modeled showing the direct band gap (green line), indirect band gap (red line), and the Urbach tail (yellow line).

CONCLUSIONS

We have demonstrated the successful use of combinatory techniques that can be used to speed up and optimize the discovery of compounds at high pressure. While being used in a low-resolution capacity, USPEX successfully guided the synthetic efforts acting as a reaction indicator of different compositions. While the predicted $GaNb_2O_5N$ oxynitride in the $GaN–Nb_2O_5$ system was not formed, the in situ EDXRD investigation mapped out the P-T reaction space in the course of a single day, leading to the discovery of two different phases having rutile and α-PbO_2 structures; analysis of phase-specific X-ray and neutron scattering data suggests that the rutile-related phase has the composition $(Nb_2O_5)_{0.84}$:$(NbO_2)_{0.32}$:$(GaN)_{0.82}$. Structural studies found that the novel oxynitride phases have positional disorder among both the cations and the anions. The incorporation of positional disorder is currently not practical with state of the art crystal structure prediction algorithms. However, while the predicted structures may not match experimental results in the current implementation of USPEX, the variable-composition calculations offer insights into the chemistry of the system and can be used to direct synthetic efforts with 0 K calculations. To increase the likelihood of success in oxynitride prediction, future directions will need to incorporate/account for disorder to better evaluate oxynitride systems.

ASSOCIATED CONTENT

Supporting Information

The Supporting Information is available free of charge on the ACS Publications website at DOI: 10.1021/acs.inorgchem.5b02791.

Experimental details of the behavior of GaN under conditions of high pressure and high temperature (HPHT), the synthesis of $NbGaO_4$ at HPHT, and details of the structure analysis obtained through refinements using X-ray and neutron diffraction data, including a detailed analysis of peak shape (PDF)

AUTHOR INFORMATION

Corresponding Author

*E-mail for J.B.P.: john.parise@stonybrook.edu.

Notes

The authors declare no competing financial interest.

ACKNOWLEDGMENTS

The theoretical calculations, HPHT synthesis, and analysis of the synchrotron, neutron, and optical data by W.R.W., A.R.O., G.-R.Q., and H.A.N.D. was supported by the National Science Foundation under its materials Genome Initiative, Grant DMR-1231586. The use of the National Synchrotron Light Source, Brookhaven National Laboratory, was supported by the U.S. Department of Energy, Office of Science, Office of Basic Energy Sciences, under Contract No. DE-AC02-98CH10886. Use of the X17B2 beamline was supported by COMPRES, the Consortium for Materials Properties Research in Earth Sciences, under NSF Cooperative Agreement EAR 10-43050 and by the Mineral Physics Institute, Stony Brook University. The collection of high-resolution X-ray diffraction patterns at the Advanced Photon Source was supported by the U.S. Department of Energy, Office of Science, Office of Basic Energy Sciences, under Contract No. DE-AC02-06CH11357. The neutron scattering measurements at POWGEN were supported by the Office of Basic Energy Sciences, U.S. Department of Energy, at the Spallation Neutron Source, Oak Ridge National Laboratory, under Contract No. DE-AC05-00OR22725 with UT Battelle.

REFERENCES

(1) Demazeau, G.; Huppertz, H.; Alonso, J. A.; Pöttgen, R.; Moran, E.; Attfield, J. P. *Z. Naturforsch., B: J. Chem. Sci.* **2006**, *61*, 1457–1470.
(2) Range, K.-J. *Chem. Unserer Zeit* **1976**, *10*, 180–188.
(3) Huppertz, H. *Chem. Commun.* **2011**, *47*, 131–140.
(4) Badding, J. V.; Meng, J. F.; Polvani, D. A. *Chem. Mater.* **1998**, *10*, 2889–2894.
(5) Gregoryanz, E.; Sanloup, C.; Somayazulu, M.; Badro, J.; Fiquet, G.; Mao, H.-k.; Hemley, R. J. *Nat. Mater.* **2004**, *3*, 294–297.
(6) Zhang, W.; Oganov, A. R.; Goncharov, A. F.; Zhu, Q.; Boulfelfel, S. E.; Lyakhov, A. O.; Stavrou, E.; Somayazulu, M.; Prakapenka, V. B.; Konopkova, Z. *Science* **2013**, *342*, 1502–1505.
(7) Lazicki, A.; Goncharov, A. F.; Struzhkin, V. V.; Cohen, R. E.; Liu, Z.; Gregoryanz, E.; Guillaume, C.; Mao, H. K.; Hemley, R. J. *Proc. Natl. Acad. Sci. U. S. A.* **2009**, *106*, 6525–6528.
(8) Eremets, M. I.; Trojan, I. A. *JETP Lett.* **2009**, *89*, 174–179.
(9) Oganov, A. R.; Ma, Y.; Lyakhov, A. O.; Valle, M.; Gatti, C. *Rev. Mineral. Geochem.* **2010**, *71*, 271–298.
(10) Oganov, A. R.; Glass, C. W. *J. Phys.: Condens. Matter* **2008**, *20*, 064210.
(11) Oganov, A. R.; Chen, J.; Gatti, C.; Ma, Y.; Ma, Y.; Glass, C. W.; Liu, Z.; Yu, T.; Kurakevych, O. O.; Solozhenko, V. L. *Nature* **2009**, *457*, 863–867.
(12) Ma, Y.; Eremets, M.; Oganov, A. R.; Xie, Y.; Trojan, I.; Medvedev, S.; Lyakhov, A. O.; Valle, M.; Prakapenka, V. *Nature* **2009**, *458*, 182–185.
(13) Solozhenko, V. L.; Solozhenko, E. G.; Zinin, P. V.; Ming, L. C.; Chen, J.; Parise, J. B. *J. Phys. Chem. Solids* **2003**, *64*, 1265–1270.
(14) Maddox, J. *Nature* **1988**, *335*, 201–201.
(15) DiSalvo, F. J. *Science* **1990**, *247*, 649–655.
(16) Glass, C. W.; Oganov, A. R.; Hansen, N. *Comput. Phys. Commun.* **2006**, *175*, 713–720.
(17) Hautier, G.; Fischer, C.; Ehrlacher, V.; Jain, A.; Ceder, G. *Inorg. Chem.* **2011**, *50*, 656–663.
(18) Wu, Y.; Lazic, P.; Hautier, G.; Persson, K.; Ceder, G. *Energy Environ. Sci.* **2013**, *6*, 157–168.

DOI: 10.1021/acs.inorgchem.5b02791
Inorg. Chem. 2016, 55, 3384–3392

(19) Curtarolo, S.; Morgan, D.; Persson, K.; Rodgers, J.; Ceder, G. *Phys. Rev. Lett.* **2003**, *91*, 135503.
(20) Demazeau, G. *Z. Naturforsch., B: J. Chem. Sci.* **2006**, *61*, 799−807.
(21) Fuertes, A. *Dalton Trans.* **2010**, *39*, 5942−5948.
(22) Maeda, K.; Domen, K. *J. Phys. Chem. C* **2007**, *111*, 7851−7861.
(23) Maeda, K.; Domen, K. *MRS Bull.* **2011**, *36*, 25−31.
(24) Maeda, K.; Teramura, K.; Domen, K. *J. Catal.* **2008**, *254*, 198−204.
(25) Tassel, C.; Kuno, Y.; Goto, Y.; Yamamoto, T.; Brown, C. M.; Hester, J.; Fujita, K.; Higashi, M.; Abe, R.; Tanaka, K.; Kobayashi, Y.; Kageyama, H. *Angew. Chem., Int. Ed.* **2015**, *54*, 516−521.
(26) Troyanchuk, I. O.; Kasper, N. V.; Mantytskaya, O. S.; Shapovalova, E. F. *Mater. Res. Bull.* **1995**, *30*, 421−425.
(27) Yang, M.; Rodgers, J. A.; Middler, L. C.; Oro-Sole, J.; Jorge, A. B. n.; Fuertes, A.; Attfield, J. P. *Inorg. Chem.* **2009**, *48*, 11498−11500.
(28) Soignard, E.; Machon, D.; McMillan, P. F.; Dong, J.; Xu, B.; Leinenweber, K. *Chem. Mater.* **2005**, *17*, 5465−5472.
(29) Kinski, I.; Miehe, G.; Heymann, G.; Theissmann, R.; Riedel, R.; Huppertz, H. *Z. Naturforsch., B: Chem. Sci.* **2005**, *60*, 831−836.
(30) Huppertz, H.; Hering, S. A.; Zvoriste, C. E.; Lauterbach, S.; Oeckler, O.; Riedel, R.; Kinski, I. *Chem. Mater.* **2009**, *21*, 2101−2107.
(31) Hering, S. A.; Zvoriste, C. E.; Riedel, R.; Kinski, I.; Huppertz, H. *Z. Naturforsch., B: J. Chem. Sci.* **2009**, *64*, 1115−1126.
(32) Chen, H.; Wang, L.; Bai, J.; Hanson, J. C.; Warren, J. B.; Muckerman, J. T.; Fujita, E.; Rodriguez, J. A. *J. Phys. Chem. C* **2010**, *114*, 1809−1814.
(33) Haines, J.; Chateau, C.; Léger, J. M.; Le Sauze, A.; Diot, N.; Marchand, R.; Hull, S. *Acta Crystallogr., Sect. B: Struct. Sci.* **1999**, *55*, 677−682.
(34) Baumann, D.; Sedlmaier, S. J.; Schnick, W. *Angew. Chem., Int. Ed.* **2012**, *51*, 4707−4709.
(35) Li, Q.; Ma, Y.; Oganov, A. R.; Wang, H.; Wang, H.; Xu, Y.; Cui, T.; Mao, H.-K.; Zou, G. *Phys. Rev. Lett.* **2009**, *102*, 175506.
(36) Oganov, A. R.; Ma, Y.; Xu, Y.; Errea, I.; Bergara, A.; Lyakhov, A. O. *Proc. Natl. Acad. Sci. U. S. A.* **2010**, *107*, 7646−7651.
(37) Zhou, X.-F.; Oganov, A. R.; Qian, G.-R.; Zhu, Q. *Phys. Rev. Lett.* **2012**, *109*, 245503.
(38) Bazhanova, Z. G.; Oganov, A. R.; Gianola, O. *Phys.-Usp.* **2012**, *55*, 489−497.
(39) Zeng, Q.; Peng, J.; Oganov, A. R.; Zhu, Q.; Xie, C.; Zhang, X.; Dong, D.; Zhang, L.; Cheng, L. *Phys. Rev. B: Condens. Matter Mater. Phys.* **2013**, *88*, 214107.
(40) Zhu, Q.; Jung, D. Y.; Oganov, A. R.; Glass, C. W.; Gatti, C.; Lyakhov, A. O. *Nat. Chem.* **2012**, *5*, 61−65.
(41) Zhu, Q.; Oganov, A. R.; Lyakhov, A. O. *Phys. Chem. Chem. Phys.* **2013**, *15*, 7696.
(42) Cheng, X.; Zhang, W.; Chen, X.-Q.; Niu, H.; Liu, P.; Du, K.; Liu, G.; Li, D.; Cheng, H.-M.; Ye, H.; Li, Y. *Appl. Phys. Lett.* **2013**, *103*, 171903.
(43) Cheng, X.-Y.; Chen, X.-Q.; Li, D.-Z.; Li, Y.-Y. *Acta Crystallogr., Sect. C: Struct. Chem.* **2014**, *70*, 85−103.
(44) Zeng, Q.; Oganov, A. R.; Lyakhov, A. O.; Xie, C.; Zhang, X.; Zhang, J.; Zhu, Q.; Wei, B.; Grigorenko, I.; Zhang, L.; Cheng, L. *Acta Crystallogr., Sect. C: Struct. Chem.* **2014**, *70*, 76−84.
(45) Yang, M.; Oró-Solé, J.; Rodgers, J. A.; Jorge, A. B.; Fuertes, A.; Attfield, J. P. *Nat. Chem.* **2011**, *3*, 47−52.
(46) Attfield, J. P. *Cryst. Growth Des.* **2013**, *13*, 4623−4629.
(47) Clark, L.; Oró-Solé, J.; Knight, K. S.; Fuertes, A.; Attfield, J. P. *Chem. Mater.* **2013**, *25*, 5004−5011.
(48) Oró-Solé, J.; Clark, L.; Bonin, W.; Attfield, J. P.; Fuertes, A. *Chem. Commun.* **2013**, *49*, 2430.
(49) Oró-Solé, J.; Clark, L.; Kumar, N.; Bonin, W.; Sundaresan, A.; Attfield, J. P.; Rao, C. N. R.; Fuertes, A. *J. Mater. Chem. C* **2014**, *2*, 2212.
(50) Bischoff, A.; Grund, T.; Jording, T.; Heying, B.; Hoffmann, R. D.; Rodewald, U. C.; Pottgen, R. *Z. Naturforsch., B: Chem. Sci.* **2005**, *60*, 1231−1234.
(51) Srinivasa, S. R.; Cartz, L.; Jorgensen, J. D.; Worlton, T. G.; Beyerlein, R. A.; Billy, M. *J. Appl. Crystallogr.* **1977**, *10*, 167−171.
(52) Yashima, M.; Lee, Y.; Domen, K. *Chem. Mater.* **2007**, *19*, 588−593.
(53) Oganov, A. R.; Glass, C. W. *J. Chem. Phys.* **2006**, *124*, 244704.
(54) Oganov, A. R.; Lyakhov, A. O.; Valle, M. *Acc. Chem. Res.* **2011**, *44*, 227−237.
(55) Lyakhov, A. O.; Oganov, A. R.; Stokes, H. T.; Zhu, Q. *Comput. Phys. Commun.* **2013**, *184*, 1172−1182.
(56) Blöchl, P. E. *Phys. Rev. B: Condens. Matter Mater. Phys.* **1994**, *50*, 17953−17979.
(57) Kresse, G.; Furthmüller, J. *Phys. Rev. B: Condens. Matter Mater. Phys.* **1996**, *54*, 11169−11186.
(58) Perdew, J. P.; Burke, K.; Ernzerhof, M. *Phys. Rev. Lett.* **1996**, *77*, 3865−3868.
(59) Troullier, N.; Martins, J. L. *Phys. Rev. B: Condens. Matter Mater. Phys.* **1991**, *43*, 1993−2006.
(60) Larson, A. C.; Von Dreele, R. B. *Report LAUR 86-748*; Los Alamos National Laboratory, Los Alamos, NM, USA, 1986.
(61) Toby, B. H. *J. Appl. Crystallogr.* **2001**, *34*, 210−213.
(62) Shannon, R. D. *Acta Crystallogr., Sect. A: Cryst. Phys., Diffr., Theor. Gen. Crystallogr.* **1976**, *32*, 751−767.
(63) Reinert, A. A.; Payne, C.; Wang, L.; Ciston, J.; Zhu, Y.; Khalifah, P. G. *Inorg. Chem.* **2013**, *52*, 8389−8398.
(64) Dharmagunawardhane, H. A. N.; Woerner, W. R.; Wu, Q.; Huang, H.; Chen, X.; Orlov, A.; Khalifah, P. G.; Parise, J. B. *J. Mater. Chem. A* **2014**, *2*, 19247−19252.
(65) Blasse, G.; Buth, A. H.; Tamura, S. *J. Solid State Chem.* **1981**, *37*, 264−266.
(66) Devi, S.; Kelkar, S.; Kashid, V.; Salunke, H. G.; Gupta, N. M. *RSC Adv.* **2013**, *3*, 16817.
(67) Whitaker, M. L.; Nekvasil, H.; Lindsley, D. H.; Difrancesco, N. J. *J. Petrol.* **2006**, *48*, 365−393.
(68) Khomenko, V. M.; Langer, K.; Rager, H.; Fett, A. *Phys. Chem. Miner.* **1998**, *25*, 338−346.

DOI: 10.1021/acs.inorgchem.5b02791
Inorg. Chem. 2016, 55, 3384−3392